Queueing up for enzymatic processing: Correlated signaling through coupled degradation (Supplementary Information)

Natalie A. Cookson, William H. Mather, Tal Danino,
Octavio Mondragón-Palomino, Ruth J. Williams, Lev S. Tsimring, Jeff Hasty

SBML Model

The SBML file of the model used for this study has been archived at the BioModels Database (MODEL1111150000).

Flow Cytometry

Flow cytometry data was taken with a Becton-Dickinson LSR II Cell Analyzer, fitted with 405nm and 488nm lasers. Because a wide range of fluorescence intensities arose as inducer levels were scanned, the sensitivity (set by voltage) of photomultiplier tubes in the flow cytometer was varied from sample to sample. We calibrated the photomultiplier tubes by scanning a range of voltages for cells with a constant mean level of fluorescent protein, either YFP or CFP alone. We fit the resulting mean YFP and CFP intensity curves to piecewise-smooth functions of voltage. These functions were used to correct flow cytometry data by scaling all measurements to a common apparent voltage.

In order to be able to directly compare numbers of fluorescent proteins of YFP and CFP, we used a plasmid containing two copies of the $P_{LtetO-1}$ promoter, one driving YFP-LAA and one driving CFP-LAA (pZA11-YC-LAA). This was constructed using similar techniques to those described above. Using this strain and the assumption that the two proteins should be produced in equal mean levels due to their tandem arrangement on the same plasmid, we induced cells at various concentrations of doxycycline and measured mean fluorescence. We scaled CFP fluorescence such that the mean CFP fluorescence values at the selected induction levels were essentially the same as the corresponding YFP mean fluorescence values (difference of 0.5% in the typical mean fluorescence), and we were able to determine a conversion factor to compare YFP "arbitrary units" (AU) to CFP AU. This, combined with the Western blot data (see below) enabled the estimation of the total number of each fluorescent protein in each data set.

As another validation of the queueing theory, we compared this dual-color induction data to an almost identical plasmid, but one in which only YFP-LAA was produced from the $P_{LtetO-1}$ promoter. Interestingly, we found that the overall level of YFP fluorescence was significantly lower in the case of expression of only one of the two colors. This falls in line with queueing theory predictions. That is, in the dual-color case, the total number of tagged proteins is doubled, so ClpXP would be more overloaded than when just a single fluorescent protein type is produced. This is further evidence that over-burdening the protease can lead to coupling between the levels of two different proteins.

As described in the main text, we also compared induction curves of tagged and untagged fluorescent proteins, in an effort to determine if the queueing effect could be directly observed in induction data. This also served to demonstrate that the effects observed throughout the experiments were in fact due specifically to the abundance of tags, and not simply side effects of general over-expression. To take this data, we created two plasmids very similar to those used for the two-color study. We used the pZE24-mcs2a cloning plasmid [1], which has a kanamycin resistance marker and the hybrid $P_{lac/ara-1}$ promoter upstream of a multiple cloning site (mcs). We simply replaced the mcs with either GFP or GFP-LAA, and used this to take induction data as described in the main text.

For all flow results, a background subtraction procedure was performed on the raw data (after the voltage correction described above) to arrive at reported YFP and CFP fluorescence statistics. Using data from the experiments discussed in the main text, we defined the background mean of YFP and CFP fluorescence as that derived from cells induced with 1 mM IPTG alone (in the absence of arabinose or doxycycline). The background mean for each color was subtracted from the mean of raw data.

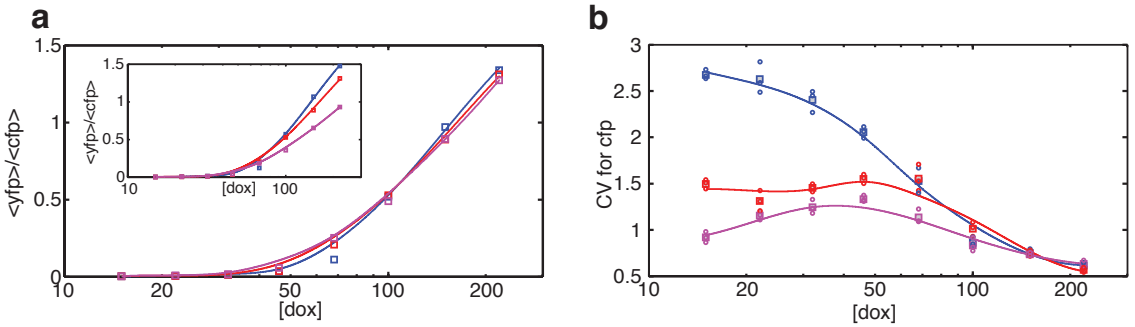

Figure S1: Coupled enzymatic degradation of yellow and cerulean LAA-tagged fluorescent proteins by ClpXP machinery in *E. coli*. (a) According to the stochastic queueing model, the ratio of the two mean concentrations $\langle x_1 \rangle / \langle x_2 \rangle$ is equal to the ratio of the corresponding production rates λ_1/λ_2. In accordance with the model, the ratio $\langle$yfp$\rangle/\langle$cfp$\rangle$ exhibits the same dependence on dox concentration for three different levels of arabinose, which allowed us to collapse all the data to a common curve by normalizing them by the mean value over the whole range of employed dox concentrations. Inset shows the same data without collapsing. (b) Coefficient of variation of CFP concentration decreases with increasing dox in the overloaded regime in qualitative agreement with the queueing theory predictions (different symbols correspond to three levels of arabinose concentration similar to panels c-d of Fig. 3 in the main text). Solid lines represent trend lines through the data.

As one further test of the stochastic queueing model, we used the theoretical results to deduce the scaling relationship between the data sets in Fig. 3c of the main text at different levels of arabinose. In other words, if correct, the theory can be used to predict how one can plot the data such that it will collapse onto the same curve. The resulting verification of this prediction further confirmed the general validity of the queueing theory approach (Fig. S1a). Lastly, we calculated the noise (as measured by the coefficient of variation) of the CFP signal as a function of increasing doxycycline (Fig. S1b). The general trend of these curves is also in agreement with the theoretical predictions.

We did not investigate the effect of removing SspB [2], a protein associated with increased affinity of tagged proteins to ClpXP. We anticipate that a moderate decrease in this Michaelis-Menten affinity would not qualitatively change our conclusions.

Protein Counts

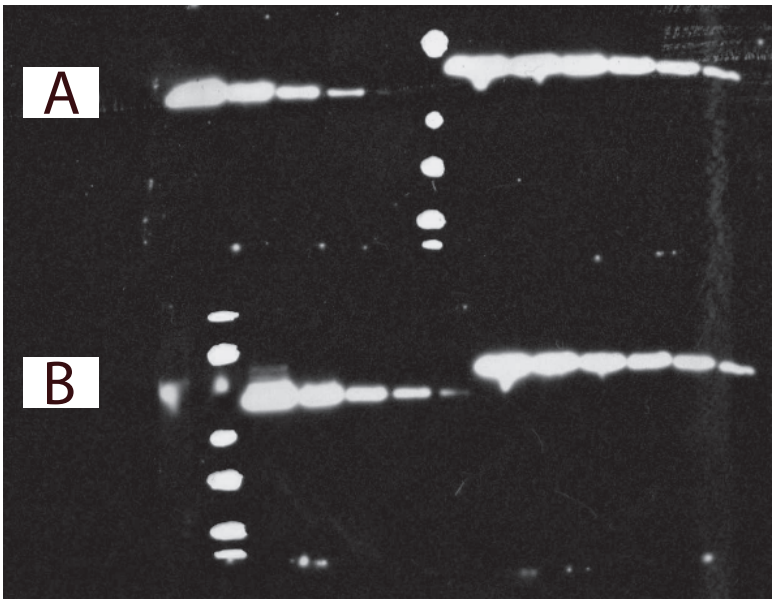

Figure S2: Inverted image of Western blot film taken for cellular lysate data from two induction levels, where IPTG and arabinose were held at 1 mM and .8%, respectively, and doxycycline was 32 ng/ml (A) and 68 ng/ml (B). An antibody for GFP variants was used to detect the total amount of CFP and YFP inside these samples, when compared to a purified GFP standard (left five lanes of both A and B).

Western blots were performed using standard techniques in order to quantify the number of tagged fluorescent proteins being measured in our flow cytometry data. As a standard, we used purified Enhanced GFP (BioVision 4999-100), supplied in a 1 mg/ml 100 μl aliquot. We chose to measure protein levels in a sample of cells expressing the pNO-2CLAA plasmid, induced to various levels of dual-color expression. For all samples, we used 1 mM of IPTG and 0.8% arabinose. Samples were induced exactly as done for the flow cytometry experiments. Cells were grown overnight without inducers, and then passed 1:1000 into inducers for 3 hours. In order to obtain enough protein for quantitative detection, 50 ml of each sample was harvested by centrifugation after 3 hours. ODs at 600 nm were taken just before centrifugation, in order to quantify cell number (see below).

After centrifuging the samples and aspirating the inducing medium, the cells were resuspended in 100 μl of SDS sample buffer to aid in cell lysis by boiling. The total volume after resuspension was measured in order to obtain an accurate measurement of cell concentration. Cells were then lysed and proteins denatured by subjecting the samples (both lysates and standards) to boiling water for 5 minutes. A 12 lane 12% Tris-Glycine gel was used in order to have enough lanes for a sufficient dilution series of both the cell lysate sample as well as the standard. The standard was diluted to a concentration of 100 ng/μl, and fives samples were loaded on the gel in subsequent 2-fold dilutions, starting with 500ng. Similarly, the cellular lysate was loaded in subsequent 2-fold dilutions, starting with a volume of 15 μl. The gel was run at 125 V for about 100 minutes, followed by a membrane transfer run at 25 V for 90 minutes.

Standard blocking and probing reactions were set up using a GFP polyclonal rabbit antibody (Cell Signaling 2555S) and an Anti-Rabbit IgG (whole molecule)-Peroxidase antibody. After exposing the membrane to the Chemiluminescent Peroxidase Substrate (Sigma, CPS-1), Kodak

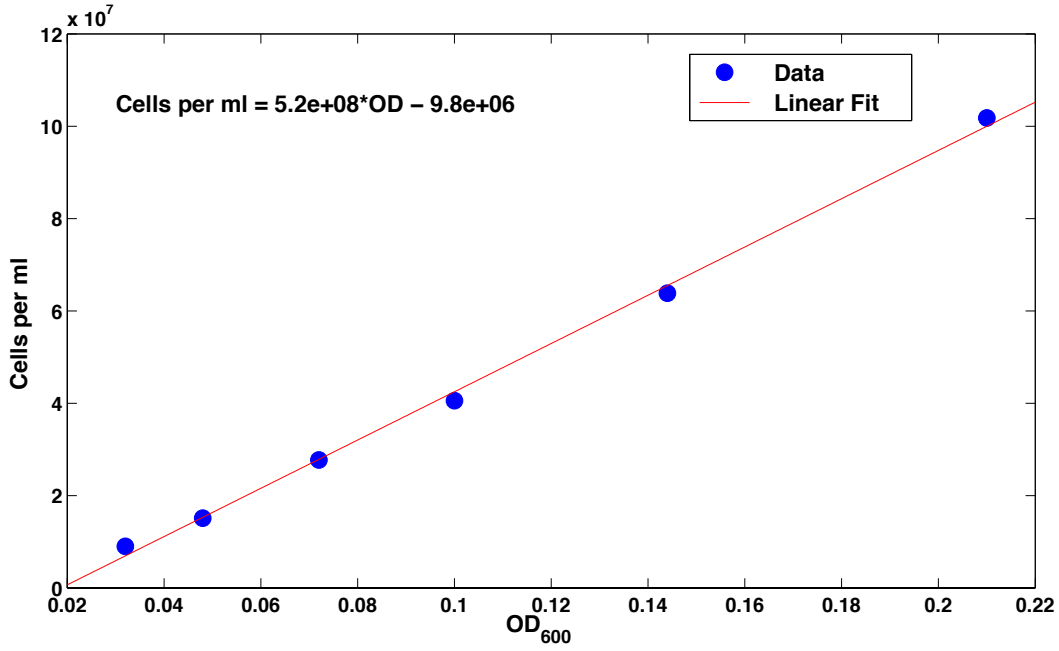

Figure S3: Cell count was correlated with OD by taking several measurements throughout logarithmic growth of each. A linear fit of this data was then used to convert the OD of Western blot samples to a particular concentration of cells.

BioMax Light Film was exposed to the membranes in a dark room for 60 seconds. Once a satisfactory image was taken, processing was performed using ImageJ. Background correction was performed to remove some of the background coloration from the image. The image was then inverted so that bands showed as white on a black background (Fig. S2), and the freehand selection tool was used to quantify the total intensity of each band. Comparing the total intensity of each standard band to the known protein mass loaded on the gel, we were able to obtain a function to convert band intensity to protein mass, and this was used to quantify several lanes of the cell lysate samples that fell within a linear range (where the known two-fold dilution matched a two-fold drop in band intensity). Finally the protein weight measurement was converted to a total protein count per cell, using the weight of a single protein and the number of cells loaded onto the gel. Control experiments were performed to ensure that this antibody binds with equal affinity to GFP, CFP, and YFP. Cells expressing each protein from the same promoter were grown in identical conditions and induced simultaneously. Western blotting was performed as described above to ensure that the same signal was detected from each of the three samples, after normalizing for cell count.

Cell counts were done using a hemacytometer. Cells were grown in inducing conditions and sampled every 20 minutes over a 3 hour period around the OD sampled for the Western blot data. Cell count was plotted vs OD over this range and a good linear fit was achieved (Fig. S3). Using this linear fit, we were able to calculate cell count for the ODs at which our cultures were sampled for the Western blots.

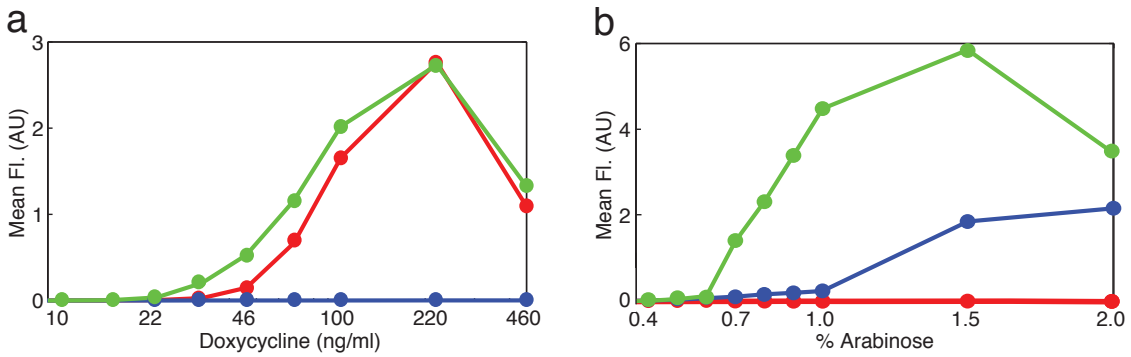

Figure S4: Control experiments were performed to ensure that there was no cross-talk between the inducers. (a) Doxycycline is shown to not induce the expression of CFP (blue), but induces YFP (red). Addition of arabinose increases YFP expression (green) due to slower overall ClpXP processing. (b) Arabinose does not induces expression of YFP (red), but induces CFP (blue). Addition of doxycycline increase CFP expression (green).

Experimental Controls

Several control experiments were performed to ensure that the coordinated behavior in our two experimental systems was due to degradation-based coupling and not just an artifact due to some other phenomenon. First, the comparison of the tagged and untagged induction curves in the main text served to demonstrate that the effects we are seeing are due to the tag and not just side effects of over-expression. In the case of the dual-tunable signaling network, another primary concern was ensuring that the two inducers did not interfere with the other promoters (i.e. that there is no cross-talk between the two promoters). To test this, we induced cells with each of the two inducers independently, and ensured that each color was only induced by the appropriate inducer (Fig. S4). In panel a, it is clear that doxycycline strongly induces YFP (red) and not CFP (blue). When arabinose is introduced in addition to doxycycline, the YFP levels increase (green), as CFP is now being produced as well, causing an increased burden on ClpXP. The reverse is true as well; in panel b, arabinose alone is seen to induce CFP (blue) and not YFP (red), however the addition of doxycycline causes increased levels of CFP. This is further evidence of queueing theory, in addition to a good control for crosstalk between the two promoters.

A similar control was performed for the dual-color synthetic circuit experiment. That is, the oscillator strain was induced with AHL, and we saw no effect on period of the oscillator, indicating that AHL and LuxR do not interfere with the ara/lac promoter. As another general control that the addition of tagged proteins causes the observed effect, as opposed to it being some other artifact of over expression, we tested the synthetic oscillatory system in conjunction with a high level of a general, untagged protein (for this purpose, we used Pn25 driving TetR, untagged on a p15A plasmid). When producing a large amount of untagged TetR (approximately 100,000 copies per cell [1]) alongside the oscillator, we saw no difference between this and the normal behavior of the oscillator. This control provides evidence that there is no apparent effect on period when expressing untagged proteins. In addition, the experimental acquisition of the two induction curves (described above), with the tagged and untagged versions of GFP, served to demonstrate that the effects observed throughout the experiments were in fact due specifically to the abundance of tags, and not simply side effects of general over-expression.

Stochastic Theory - Model

The model considered in this paper involves production and degradation of protein types X_i, where indices $i = 1, 2, ..., m$ identify different protein types. Degradation occurs by the protein binding to a protease P and subsequently being annihilated. Specifically, the model reactions are (rates are rate constants, not including mass action terms)

$$D_i \xrightarrow{\lambda_i} X_i + D_i \tag{1}$$

$$X_i \xrightarrow{\gamma} \emptyset \tag{2}$$

$$X_i + P \underset{\eta_-}{\overset{\eta_+}{\rightleftharpoons}} X_i P \tag{3}$$

$$X_i P \xrightarrow{\mu} P \tag{4}$$

$$X_i P \xrightarrow{\gamma} P \tag{5}$$

where DNA D_i produces protein X_i with rate constant λ_i, X_i is diluted (due to cell growth and division) with rate constant γ, X_i binds to the protease P with rate constant η_+, X_i unbinds from P with rate constant η_-, and P degrades X_i with rate constant μ. Reactions occur with exponentially distributed times. For simplicity of results, we assume that dilution can act on X_i bound to P, though results can be generalized to when dilution does not act on X_i bound to P. We typically assume results for a single effective protease (with an exception at the end of this section), though single protease results can be generalized to many proteases [3]. We assume the count of each DNA D_i is 1 for simplicity.

Using reasonable approximations, we can further simplify Eqs. 1–5. The simplest approximation is to suppose that $\eta_- \approx 0$ and that η_+ is large, such that the reactions in Eqs. 2 and 5 collapse to Eq. 2 and Eqs. 3–4 combine into a single degradation reaction, where the protease chooses one particular protein and degrades it at rate μ; the latter has the same steady-state behavior as when Eqs. 3-4 are replaced by the reaction

$$X_i \xrightarrow{\mu/n} \emptyset \tag{6}$$

where $n = \sum_{j=1}^{m} x_j$, and x_i is the count of protein type X_i, as in the main text. Similar results can be derived if both η_+ and η_- are sufficiently large. This leads instead to the approximate degradation reaction

$$X_i \xrightarrow{\mu/(K+n)} \emptyset \tag{7}$$

where $K = \eta_-/\eta_+$ is a Michaelis-Menten parameter [3]. In the limit $K \to 0$, the $\eta_- \approx 0$ system is recovered. More details concerning the motivation and derivation of the reduced rates in Eqs. 6–7 appear in Refs. [3, 4].

The reduced system, using either Eq. 6 or Eq. 7 for the enzymatic degradation reactions Eqs. 3–4, can be mapped (preserving the statistical distributions of protein counts) onto a stochastic queueing

model. One such queueing model places each new X_i at a random position in a single queue, while P processes (degrades) the protein at the head of the queue. Dilution can be added by allowing "reneging," whereby any member of the queue (including a member being processed by the server) leaves at an average rate of γ.

In Fig. 2, a version of this stochastic queueing model is used to describe the σ^s stress response system. We consider two substrates, mistranslated proteins, X_m and σ^s proteins, We suppose there are 100 ClpXP "servers" that each have processing rate $\mu = 10$ min^{-1}. Binding of both substrates to ClpXP is assumed fast ($\eta^+ = 10^8$ min^{-1}), and unbinding negligible ($\eta^- = 0$ min^{-1}). Cells are assumed to divide every 20 min, such that $\gamma = \ln 2$ min^{-1}. Production of mistranslated proteins occurs with rate λ_m, and the production of σ^s occurs with rate λ_{σ^s}. The system is overloaded when $\lambda_m + \lambda_{\sigma^s} > 100\,\mu$, balanced when $\lambda_m + \lambda_{\sigma^s} = 100\,\mu$, and underloaded otherwise. The statistics presented in Fig. 2 are derived from a large 32,000 ensemble of simulations. Single trajectories also use an ensemble size of 1. Numerical simulations take advantage of custom code using the CUDA framework for GPU acceleration.

Stochastic Theory - Results

We have carefully derived several relevant results for the above model in another study [3], which applies the theory of multiclass queueing in the context of gene regulation. One key result is that the steady state probability distribution $P(\{x_i\})$ for the set of counts $\{x_i\}$ can be factored into $R(n)$, the probability distribution for the sum, times a multinomial distribution:

$$P(\{x_i\}) = R(n)\, n! \prod_{j=1}^{m} \frac{p_j^{x_j}}{x_j!} \tag{8}$$

where $p_i \equiv \lambda_i / \sum_{j=1}^{m} \lambda_j$. From this, it can be shown that moments of x_i are given in terms of moments of n. In particular,

$$\langle x_i \rangle = p_i \langle n \rangle \tag{9}$$

$$\sigma_i^2 \equiv \langle x_i^2 \rangle - \langle x_i \rangle^2 = p_i(1-p_i)\langle n \rangle + p_i^2(\langle n^2 \rangle - \langle n \rangle^2) \tag{10}$$

The moments of n are less general and will depend on the particular model. With the reaction scheme Eqs. 1–2, 7, we find

$$\langle n \rangle = \frac{\alpha\delta M(\alpha+1, \beta+1, \delta)}{\beta M(\alpha, \beta, \delta)} \tag{11}$$

$$\langle n^2 \rangle = \langle n \rangle + \frac{\alpha\,(\alpha+1)\delta^2}{\beta\,(\beta+1)} \frac{M(\alpha+2, \beta+2, \delta)}{M(\alpha, \beta, \delta)} \tag{12}$$

with $\alpha \equiv K+1$, $\beta \equiv (\mu/\gamma) + \alpha$, $\delta \equiv \Lambda/\gamma$, $\Lambda \equiv \sum_{i=1}^{m} \lambda_i$, and $M(\,\cdot\,,\,\cdot\,,\,\cdot\,)$ the confluent hypergeometric function of the first kind.

Deterministic Approximation for Mean Protein Counts

Though deterministic models do not address the many issues tied to noisy dynamics, e.g. correlations between the counts of the protein species, certain aspects of queueing coupling can be understood using a deterministic analog of the stochastic queueing model. Deriving approximately deterministic processes from chemical reaction networks has a long history, and so we will be brief

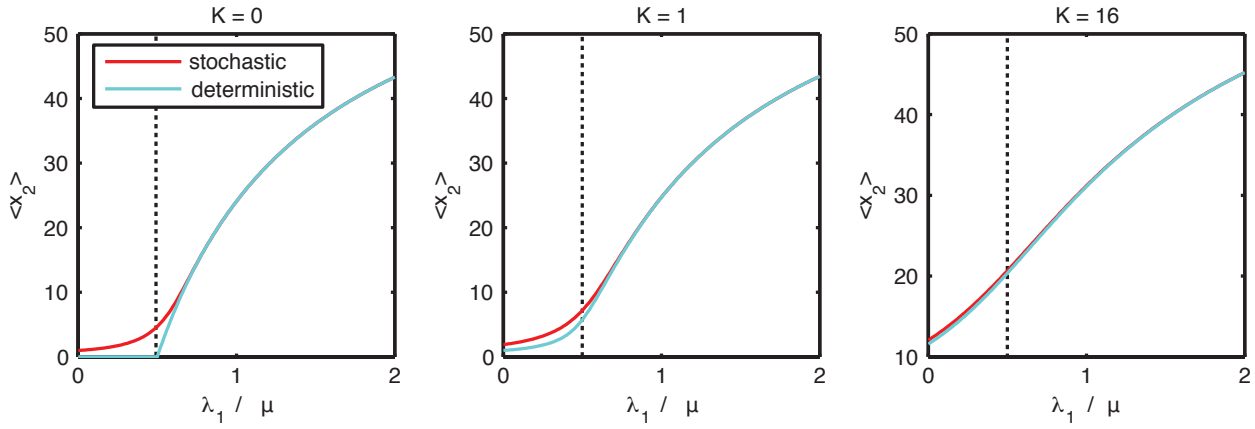

Figure S5: The deterministic approximation at steady state (see Eq. 13) can reasonably approximate the mean concentration of proteins for the stochastic model at steady state, especially when the system is above balance or when the Michaelis-Menten constant K is nonzero. Shown are results for a stochastic model and its deterministic approximation for a system containing one enzyme with processing rate $\mu = 100$ (AU). Proteins of type 2 are produced at constant rate $\lambda_2 = 0.5\,\mu$, and dilution occurs with rate $g = \ln 2$. The indirect response of mean protein level $\langle x_2 \rangle$ is plotted as a function of the normalized production rate λ_1/μ of protein 1. It is seen that deviation of the deterministic approximation from the stochastic mean value is largest in the underloaded regime (left of the dashed line) and smallest in the overloaded regime (right of the dashed line). Furthermore, increasing K reduces the error in the underloaded regime. These results support the general trend that we find in our analysis.

in the details of this section. We use this deterministic approximation primarily to accelerate some of our model fitting routines, but final results in the main text are always derived from stochastic models.

A deterministic approximation for mean protein levels x_i in a stochastic model with multiple servers is given by

$$\frac{dx_i}{dt} = \lambda_i - \gamma x_i - \frac{\mu x_i}{K + n} \tag{13}$$

where λ_i is a production rate constant, γ is the dilution rate constant, K is a Michaelis-Menten molar constant, μ is the total enzymatic processing rate constant, and $n = \sum_{j=1}^{m} x_j$ is the mean total protein count over all types. See [5] for mathematical details of derivation and validity for similar systems. By comparison to numerical simulations, the deterministic model is a reasonable approximation for the *mean* protein levels of the stochastic model (see Fig. S5). Deviation between the deterministic model and stochastic mean levels is largest in the balanced and underloaded regimes, but this deviation tends to be small when compared to the scale μ/γ, especially when the constant K is nonzero.

The steady state solutions $x_i^{(ss)}$ to Eqs. 13 satisfy a relation similar to Eq. 9

$$x_i^{(ss)} = p_i n^{(ss)} \tag{14}$$

where $n^{(ss)}$ is the total protein at steady state, and $p_i \equiv \lambda_i/\Lambda$. For finite K

$$n^{(ss)} = \frac{\Lambda - \mu - K\gamma + \sqrt{(\Lambda - \mu)^2 + K\gamma(2\Lambda + 2\mu + K\gamma)}}{2\gamma} \tag{15}$$

which simplifies in the limit $K \to 0$ to

$$n^{(ss)} = \frac{\Theta(\zeta)}{\gamma} \tag{16}$$

where $\zeta = \Lambda - \mu$, and $\Theta(\cdot)$ is the integrated Heaviside step function: $\Theta(\zeta) = \zeta$ if $\zeta \geq 0$ and $\Theta(\zeta) = 0$ if $\zeta < 0$. The solutions in Eqs. 14–16 reveal that components strongly interact when at least two λ_i's are simultaneously nonzero and $\Lambda > \mu$.

Fitting of Steady State Model

Figs. 3b–d in the main text include fits of the stochastic model to the data. Below, we outline the procedure to obtain fitted model parameters.

The fitted model results presented in Figs. 3c–d of the main text were derived through use of a fitting algorithm to determine model parameters μ, γ, K, a Hill function parameterization for λ_1 (production rate of YFP for a given dox level), and a set of 3 values for λ_2 (production rate of CFP for a given arabinose level). At the end of this section, we revisit these best fit values of λ_2 to find they are in reasonable agreement with single fluorescent protein expression data.

Curve fitting was implemented by a Metropolis algorithm. The energetic penalty used for the algorithm was a weighted sum of the square distances between stationary state model mean values (see Eqs. 9 and 11) and mean fluorescence data points. Due to the wide range of YFP fluorescence magnitudes, we used linear distance when comparing CFP fluorescence and logarithmic distance when comparing YFP fluorescence.

Parameters γ and K were not especially important for our fitting. We scaled time by the doubling time τ_d (approximately 30 min.), such that the value of the dilution rate was fixed at $\gamma = \ln 2$ in natural units. Furthermore, we set $K = 0$ with little reduction in the goodness of fit, and setting $K \leq 1000$ or so did not drastically change the results.

We found that the deterministic queueing model's stationary state approximates the overloaded stochastic queueing model's mean values well, and so we used the deterministic model's results for rapid fitting of the data, even though final results are generated from the stochastic model. Arbitrary precision calculations in the Maple 11 software package (Waterloo Maple Inc.) confirmed the stochastic model's mean values were reasonably approximated by the deterministic model with the assumption of overloading.

Using the data from the dox induction curves in Figs. 3c–d of the main text, λ_1 was fit to a shifted Hill function of the form

$$\lambda_1 = B_1 + D_1 \frac{(([\text{dox}]/C_1)^{H_1})}{(1 + ([\text{dox}]/C_1)^{H_1})}. \tag{17}$$

with $H_1 = 3.0782$, $B_1/\mu = 0.0023$, $D_1/\mu = 2.3429$, and $C_1 = 168.2114$ ng/mL. We did not fit λ_2 to a smooth curve, due to a small number of points being available, but we found best fit values $\lambda_2/\mu = 1.0373$, 1.1093, 1.2683.

Other parameters used for Figs. 3c–d in the main text are as follows: Using doubling time $\tau_d \approx 30$ min (for *E. coli*), $\mu = 7.589 \times 10^3$ min^{-1}, $\gamma = \ln 2$, $K = 0$.

We tested consistency of the model fit in Figs. 3c–d by comparing results to the data in Fig. 3b. Here, we found a continuous curve fit for the mean untagged (slow degrading) GFP fluorescence multiplied by γ, providing a continuous parameterization of the apparent production rate of GFP. Before fitting, to account for the difference between single molecule GFP and CFP fluorescence, we scaled GFP fluorescence such that the three values of mean CFP fluorescence at low dox (in

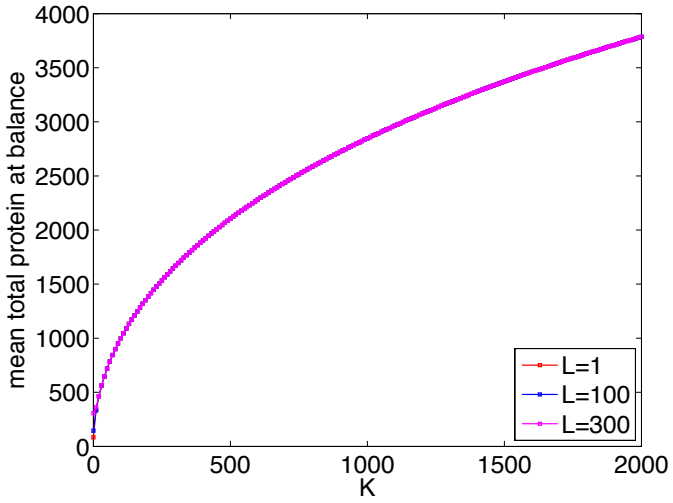

Figure S6: Pictured is the mean total protein at balance for the stochastic queueing model over a range of the Michaelis-Menten constant K. This is approximated here by each protease (copy number L) processing at a reduced rate μ/L and with Michaelis-Menten constant K. The balanced condition is defined here as when the total protein production rate Λ equals the total processing rate μ, i.e. $\Lambda = \mu$. Other parameters are determined from the model fit in this section. We find the mean total protein at balance depends weakly on L for $K > 0$. The theoretical protein level at $K = 1000$ can be considered a moderate perturbation compared to the typical protein level for the experimental data in Fig. 3 of the main text. Note that even for zero K, queue lengths are nonzero.

Figs. 3c–d) were closest in a least squares sense to the corresponding mean GFP fluorescences. We fit the apparent production rate $\lambda_2^* = \gamma < \text{gfp} >$ to the continuous function

$$\lambda_2^* = B_2 + D_2 \frac{(([\text{ARA}]/C_2)^{H_2})}{(1 + ([\text{ARA}]/C_2)^{H_2})}. \tag{18}$$

with $H_2 = 1.3660$, $B_2/\mu = 0.0665$, $D_2/\mu = 3.1039$, and $C_2 = 1.0323$ %. The difference $\Delta\lambda_2$ between λ_2 from panels c,d and λ_2^* from panel b are relatively minor, being $\Delta\lambda_2/\lambda_2 = 0.1093, 0.0144, -0.0850$, respectively, suggesting that the fits are consistent.

In Fig. 3b, using the parameterization λ_2^* and the model parameters determined by Fig. 3c–d, we present the prediction for mean protein count as a solid red curve. This prediction is in agreement with the data in Fig. 3b, suggesting that the data in Fig. 3b and in Figs. 3c–d are in agreement.

Though we found a small value of K (e.g. about a thousand or less) was consistent with our model fit, the effect of larger K on the stochastic queueing model at the balance point was considered (see Fig. S6).

References

[1] R. Lutz and H. Bujard. Independent and tight regulation of transcriptional units in *Escherichia coli* via the LacR/O, the TetR/O and AraC/I_1-I_2 regulatory elements. *Nucleic Acids Res.*, 25(6):1203–10, Mar 1997.

[2] I. Levchenko, M. Seidel, R. T. Sauer, and T. A. Baker. A specificity-enhancing factor for the ClpXP degradation machine. *Science*, 289(5488):2354–6, Sep 2000.

[3] W.H. Mather, N.A. Cookson, J. Hasty, L.S. Tsimring, and R.J. Williams. Correlation resonance generated by coupled enzymatic processing. *Biophysical Journal*, 99(10):3172–3181, 2010.

[4] K.R. Sanft, D.T. Gillespie, and L.R. Petzold. Legitimacy of the stochastic Michaelis-Menten approximation. *IET Syst. Biol.*, 5:58–69, 2011.

[5] N.G. van Kampen. Power series expansion of master equation. *Canadian Journal Of Physics*, 39(4):551–567, 1961.